TECNIACÚSTICA
CUENCA 2023

NUMERICAL STUDY OF SYMMETRIC HEXAGONAL ACOUSTIC METASURFACE FOR SOUND TRANSMISSION LOSS UNDER NORMAL INCIDENCE

Ramos D. [1*]*; Godinho L.* [1]*; Amado-Mendes P.* [1]*; Mareze P.* [2]
[1]University of Coimbra, ARISE, ISISE, Department of Civil Engineering
[2]Federal University of Santa Maria, Department of Structures and Civil Construction, Acoustic Engineering

ABSTRACT

The interest in sound wave propagation on subwavelength regimes is a widely researched field. In this context, acoustic metamaterials have arisen as a potential source of new technologies for the development of lightweight acoustical devices in subwavelength dimensions. Previously research has evidenced the capacity of symmetric acoustic systems to achieve impressive acoustical behaviours, as an example, perfect sound absorption in wide broadband, enabled by the critical coupling of resonators with distinct resonances in symmetric axially located system. This work, analyses the sound transmission loss in these system types, through a finite element model. The objective of this research is to understand the applicability of these devices in the development of compact attenuators with potential application in different contexts of engineering, especially on ventilated systems in buildings.

Keywords **–** Acoustic metamaterials, sound transmission loss, passive ventilation, Helmholtz resonators.

1. INTRODUCTION

In acoustics, the interest in manipulating the sound wave propagation at low-frequencies has been the target of several scientific studies, and, in recent years, several attempts have been made in the development of acoustic metamaterials for that purpose, enabling non-natural physical behaviours. As a result, the usage of a Helmholtz resonator for the development of these tailored systems due to their resonant behaviours can deal with the dissipative effects at audible frequencies below 1kHz, originating new approaches, such as the broadband absorbing materials [1,2]; improvements of sound insulation [3]; acoustic cloaking [4]; acoustic black hole [5]; vibration dampening [6], possible by locally resonant elements theory.

Previous research [1] considers the axial coupling of locally resonant structures to achieve wideband perfect sound absorption; however, it does not extend to the sound transmission properties. Thus, through finite element models, the authors expand these developments to sound transmission loss analyses. A brief validation of the finite element model is performed through an analytical description using the fluid equivalent Johnson-Champoux-Allard model for rigid frame [7], and a Transfer Matrix approach. Then, experimental evaluation was done using a simplified Three-Microphone impedance tube approach [8] to retrieve the normal Sound Transmission Loss (nSTL). Finally, a symmetric acoustic metamaterial composed of axially coupled Helmholtz resonators tuned for different frequencies is studied to propose a strategy to achieve an improved transmission loss.

This article is organized as follows: In section 2, the authors propose the acoustical metasurface and the respective geometrical descriptions. Then, in section 3, the involved mathematical models and methods of evaluation are described, as well as a brief analytical description of the viscous thermal losses involved, the finite element description, and a brief experimental description of the validation method using a three-microphone approach. Finally, the adopted theoretical models will be discussed, with the main conclusions summarized in section 5.

2. DESIGN AND MATHEMATICAL DESCRIPTION OF THE ACOUSTIC METASURFACE

2.1. Geometrical description

Figure 1 presents a scheme of the proposed acoustic metasurface, as illustrated in Figure 1(a), composed of n hexagonal meta unitary cells, as illustrated in Figure 1(b). Thus, the symmetric system is composed of six Helmholtz resonators, axially coupled in a waveguide with a cross-sectional radius r_w and length l_w.

Consider the Helmholtz resonator, with the neck dimensions given by, $l_{neck}^{[n]}$ and $w_{neck}^{[n]}$, corresponding to the length and the width, respectively, and the superscript $[n]$ being the order of the included resonator. By mathematical simplification, consider the resonant cavity as a parallelepiped, with length and width, $l_{cav}^{[n]}$and $w_{cav}^{[n]}$, respectively. In this system, assume that the acoustic waves propagate in the same direction as the z axis of the waveguide, the discontinuity between the acoustic field of radius r_t, and the waveguide of radius r_w is accounted for, resulting in an alteration in the fluid velocity.

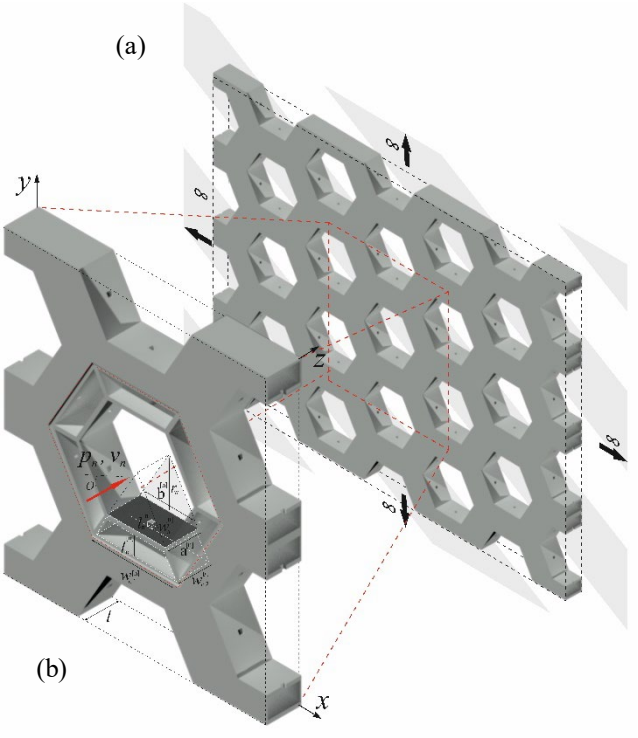

Figure 1. (a) The conceptual proposition of infinite acoustic metasurface. (b) Schematic view of a unit cell.

3. EVALUATION METHODS

3.1. Viscous thermal losses

It is important to understand that the dissipative losses in narrow channelled cross-sections play a significant role in the acoustic description and mathematical modelling of acoustic systems. The viscothermal losses in the resonator's parts can be accounted for by equivalent complex quantities, e.g. effective mass density ρ_{eff} [9] and effective bulk modulus B_{eff} [10], described as follows:

$$\rho_{eff}(\omega) = \rho_0 \alpha_\infty \left(1 + \frac{\phi\sigma}{\mathrm{j}\omega\rho_0\alpha_\infty}\left(1 + \mathrm{j}\frac{4\omega\rho_0\eta\alpha_\infty^2}{\sigma^2\phi^2\Lambda^2}\right)^{\frac{1}{2}}\right), \quad (1)$$

$$B_{eff}(\omega) = \frac{\gamma P_0}{\gamma - (\gamma-1)\left(1 + \frac{8\eta}{\mathrm{j}\omega \mathrm{Pr}\rho_0\Lambda'^2}\left(1 + \mathrm{j}\frac{\omega \mathrm{Pr}\rho_0\Lambda'^2}{16\eta}\right)^{\frac{1}{2}}\right)^{-1}}. \quad (2)$$

The description of the viscous effects inside the inlet hole as well as the acoustic fluid distortion in the outer rigid layer are strictly controlled by the specific airflow resistivity, given by [7]:

$$\sigma = \left(\frac{2\,l_n}{r_h} + 4\right)\frac{R_s}{\phi}\frac{1}{l_n}; \quad (3)$$

being, ϕ, the porosity is equal to 1 [-]; the resistive term, R_s, is the surface resistance, which corresponds to the flux distortion dependent on the angular frequency ω, expressed by [7]:

$$R_s = \frac{\sqrt{2\eta\omega\rho_0}}{2}. \quad (4)$$

The distortion of the acoustic flow due to the sudden change in cross-section associated with the inertial load due to sound radiation, expresses the reactive portion, through the geometric tortuosity, $\alpha_\infty = 1$, the thermal and viscous characteristics lengths, Λ and Λ', are numerically equal to the hydraulic radius, $r_n = w_n/\sqrt{\pi}$.

Consequently, for analytical considerations, the transfer matrix $\mathbf{T}$ expresses the relationship between the parts of the system, in the initial moment, p_1 and v_1, respectively, to the final moment, p_2 and v_2, with the assembly of matrix elements being written by:

$$\mathbf{T}\begin{bmatrix} p_1 \\ v_1 \end{bmatrix}_{x=0} = \mathbf{T}_{\mathrm{w}}^{[n]}\mathbf{T}_{\mathrm{HR}}^{[1]}\cdots\mathbf{T}_{\mathrm{HR}}^{[n-1]}\mathbf{T}_{\mathrm{HR}}^{[n]}\mathbf{T}_{\mathrm{w}}^{[n]} = \mathbf{T}\begin{bmatrix} p_2 \\ v_2 \end{bmatrix}_{x=l}. \quad (5)$$

Here, the sound wave radiation for an arbitrary segment part of the system, herein represented by $\mathbf{T}_{\mathrm{i}}^{[n]}$, is expressed by the transfer matrix:

$$\mathbf{T}_{\mathrm{i}}^{[n]} = \begin{bmatrix} \cos(k_{\mathrm{i}}^{[n]} l_i) & \mathrm{j}Z_i^{[n]}\sin(k_i^{[n]} l_i) \\ \mathrm{j}\sin(k_i^{[n]} l_i)/Z_i^{[n]} & \cos(k_i^{[n]} l_i) \end{bmatrix}, \quad (6)$$

where $k_{\mathrm{i}}^{[n]}$ and l_{i}, are, respectively, the wavenumber and length of the waveguide, and $Z_{\mathrm{i}}^{[n]}$ is the characteristic impedance of the waveguide.

3.2. Numerical Verification

To investigate the acoustic behaviour of the proposed acoustic metamaterial (AMM), a threedimensional (3D) finite element model has been implemented with the commercial software COMSOL Multiphysics 5.3. As illustrated in Figure 2, the finite element model represents a simplified approach to retrieve the sound transmission loss under normal incidence. Initially, assuming the time-harmonic dependence ($e^{j\omega t}$), in linear regime, the periodicity condition is imposed in a two-port model, being by the respective incident and transmitted pressure fields, p_{inc} and p_{trans}.

The main domain consists of a cylindrical acoustic field, with a radius r_t, defined as air, with mass density ($\rho_0 = 1.23\ kg/m^3$), air dynamic viscosity ($\eta = 1.82\times10^{-5}$ Pa·s), and ambient pressure $P_0 = 101325$ Pa.

The acoustic excitation of the system, at the left side, is an incident plane acoustic wave of unitary amplitude (1 Pa), impinging and propagating under normal incidence, originated in a sound hard boundary (SHB). To eliminate reflections of the scattered sound waves originating from planar sound waves at normal incidence, at the end surfaces of the main domain, two perfectly matched layers (PML) are imposed, discretized with twelve elements in the z-direction. In addition, all external surfaces of the domain are defined as perfectly rigid and reflective.

The discretization of the finite element model has been performed using tetrahedral elements, as illustrated in Figure 2, with the maximum element size given by $\lambda_{min}/8$, where $\lambda_{min} = c_0/f_{max}$ is the smallest acoustic wavelength within the simulated range of frequencies, corresponding to a maximum

frequency of 1kHz, what denotes eight elements per wavelength in the discretized main domain.

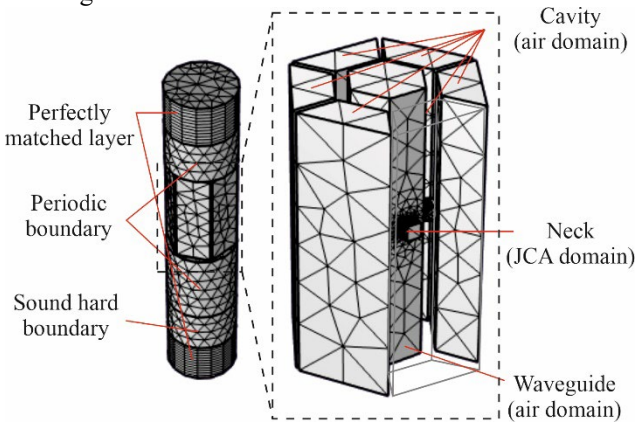

Figure 2. A finite element model discretization of the proposed AMM unit cell.

The narrow domains were modelled as three-dimensional tetrahedral elements, and their discretization was performed in parts, as follows: in the necks of the HRs, the maximum mesh size is $w_n^{[n]}/4$ and the minimum size is $d_v/2$, where $d_v = \sqrt{2\mu/\rho_0\omega}$ is the thickness of the viscous boundary layer; by simplifications, in the cavities, assuming the discontinuity of the cross-section in the volumetry, and considering the reduction of the dissipative effects inside the same, the maximum mesh size is $w_c^{[n]}/2$ and $w_c^{[n]}/4$ as the minimum mesh size.

The sound transmission loss (STL) is subsequently calculated considering the pressure level difference between the two pressure fields, according to the equation:

$$\mathrm{STL} = 20\log\left|\frac{p_{inc}}{p_{trans}}\right|. \quad (7)$$

3.3. Specimens production and experimental validation analysis

A preliminary experimental analysis has been performed within the scope of this work. Considering the dimensions of a cylindrical impedance tube of 37.5 mm inner diameter, for validation purposes of the mathematical approaches, experimental measurements of normal sound transmission loss was performed in laboratory conditions, following a simplified three-microphone transfer function approach previously described in [8], as illustrated in figure 3(a), as alternative to the standard method ASTM E2611 [11].

A printed sample AMM cell is illustrated in Figure 3(b), produced using a Blocks One 3D printer with Polylactic Acid (PLA) and equipped with a nozzle extruder with 0.4mm. This sample is intended to be experimentally evaluated according to the above mentioned three-microphone approach, alternative to the standard methodology described in ASTM E2611 [11].

(a) (b)

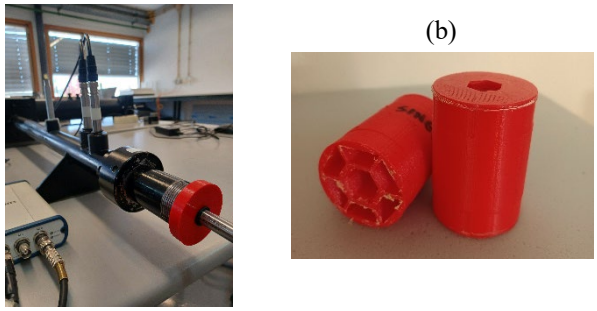

Figure 3. (a) Image of the implemented measurement setup. (b) Photograph of a printed AMM cell.

As a validation, assuming the approaches previously presented, Figure 4 shows the nSTL of the acoustic metamaterial computed using the TMM (solid lines) and the finite element method (cross markers), together with experimental measurements (circle markers).

In Figure 4, results from the three samples can be analysed; first, the grey plots represent the results considering just the waveguide, without any HRs; second, in red, the single system tuned for a resonance frequency of 950Hz can be obserevd; and, finally, the plotted blue curves correspond to HRs with a resonance frequency of 1075Hz. These results show there is good agreement between the implemented methods when computing the transmission loss properties of the AMM cell.

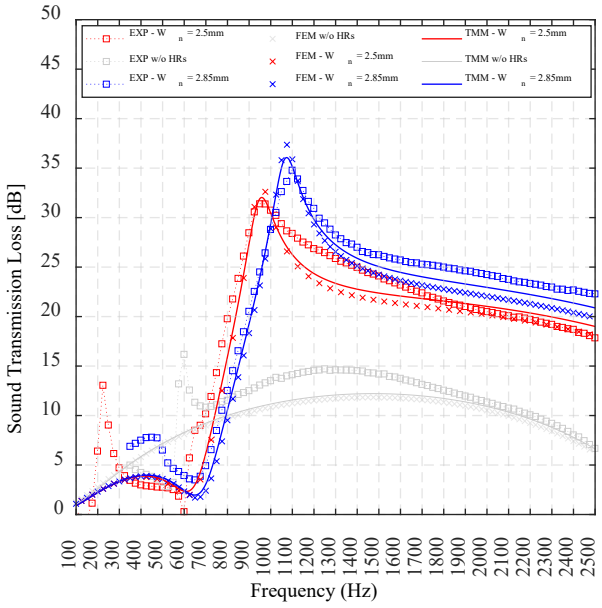

Figure 4. Validation of the nSTL for a single symmetric proposition for three approaches developed. The solid lines represent the TMM results, the cross markers the numerical results, and the square markers the experimental results, respectively.

4. RESULTS

4.1. nSTL for a single symmetric system

First, we analyse the nSTL capacity of the unit cell with six resonators attached, tuned to the same resonance frequency, f_1^{single} = 950Hz. The geometric parameters corresponding to each resonator are defined in Table 1.

Table 1. Geometrical parameters (mm) of the single HR proposition AMM.

$w_n^{[n]}$ (mm)	$l_n^{[n]}$ (mm)	$w_c^{[n]}$ (mm)	$l_c^{[n]}$ (mm)	f_l^{TL} (Hz)	f_u^{TL} (Hz)	f_{range} (Hz)
2.5	2.5	21	10	840	2300	950

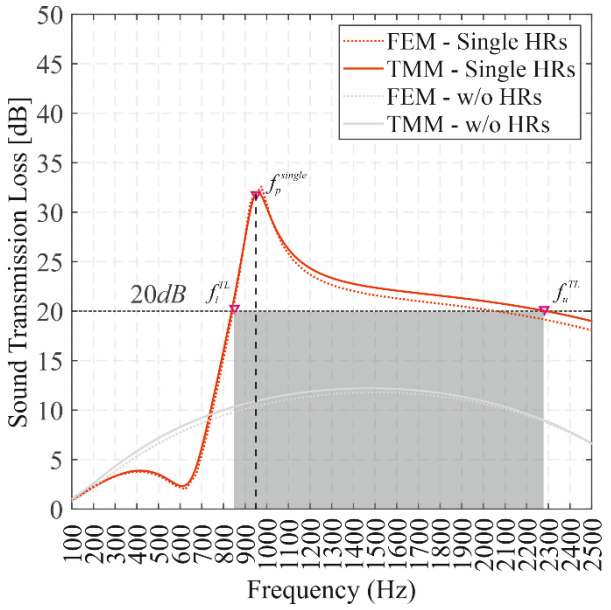

Figure 5. Evaluation of the nSTL for a single symmetric proposition for one resonant frequency $f_1 = 950$ Hz. The solid lines represent the TMM results, and the dotted lines the numerical FEM results, respectively.

Figure 5 presents the results of normal sound transmission loss, with the numerical and analytical approaches, observing the highest values of the nSTL of around 30dB at the specified frequency. It is interesting to note that a nSTL above 20dB (black dashed line), in the interval of $f_l^{TL} = 835Hz$ for the lower bound and $f_u^{TL} = 2295Hz$ for the upper bound, can be observed.

The values obtained by numerical prediction and analytical approaches present good agreement. Given the possibility of axial coupling of HRs in different geometric configurations, next, two different designs will be proposed to study the possibility of expanding the frequency band without varying the total thickness of the structure.

4.2. Normal sound transmission loss for the multi-resonance proposition

In this section, in order to illustrate the effect of coupled resonances in axial devices, initially, we present a proposal for double resonance effect, in Figure 6. Here, considering the coupling of the set of three identical resonators tuned at two resonance frequencies, at f_1^{dual} = 950 Hz and f_2^{dual} = 1200 Hz, respectively, with the geometric parameters defined in Table 2.

Table 2. Geometrical parameters (mm) of the dual HR proposition AMM.

$w_n^{[n]}$ (mm)	$l_n^{[n]}$ (mm)	$w_c^{[n]}$ (mm)	$l_c^{[n]}$ (mm)	f_l^{TL} (Hz)	f_u^{TL} (Hz)	f_{range} (Hz)
2.5	2.5	21	10	875	2425	950
32	2.5	21	10			1200

Figure 6 presents the nSTL calculated through the two mathematical approaches previously described. Again, in this plot, the grey shade indicates the frequency range for which a minimum nSTL of around 20dB is obtained. It is evident that when the coupling of a set of HRs tends to reduce the transmission peaks, however, this effect does not affect the overall transmission loss of the system, increasing the interval with nSTL>20dB to a range of $f_l^{TL} = 835Hz$ for the lower bound and $f_u^{TL} = 2450Hz$ for the upper bound.

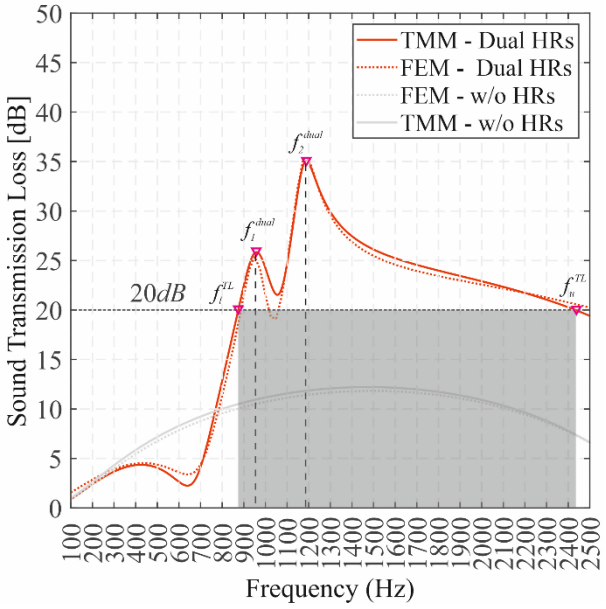

Figure 6. Evaluation of the nSTL for a dual symmetric proposition for two different frequencies $f_1 = 950$ Hz and $f_2 = 1200$Hz. The solid lines represent the TMM results, and the dotted lines the numerical results, respectively.

Finally, in the third case, the coupling between three resonant frequencies, $f_1^{triple} = 950Hz$, $f_2^{triple} = 1200Hz$

and $f_3^{triple} = 1425Hz$, respectively, with the geometric parameters defined in table 2 is analyzed.

Table 3. Geometrical parameters (mm) of the triple HR proposition AMM.

$w_n^{[n]}$ (mm)	$l_n^{[n]}$ (mm)	$w_c^{[n]}$ (mm)	$l_c^{[n]}$ (mm)	f_l^{TL} (Hz)	f_u^{TL} (Hz)	f_{range} (Hz)
2.5	2.5	21	10	890	~3000	950
3.2	2.5	21	10			1200
4.0	2.5	21	10			1425

Figure 7 presents the results of normal sound transmission loss, for the numerical and analytical approaches. Considering, again, a minimum nSTL around 20dB (black dashed line), it is possible to observe that this value is attained at frequencies between $f_l^{TL} = 875Hz$ and f_u^{TL} higher than 2500Hz.

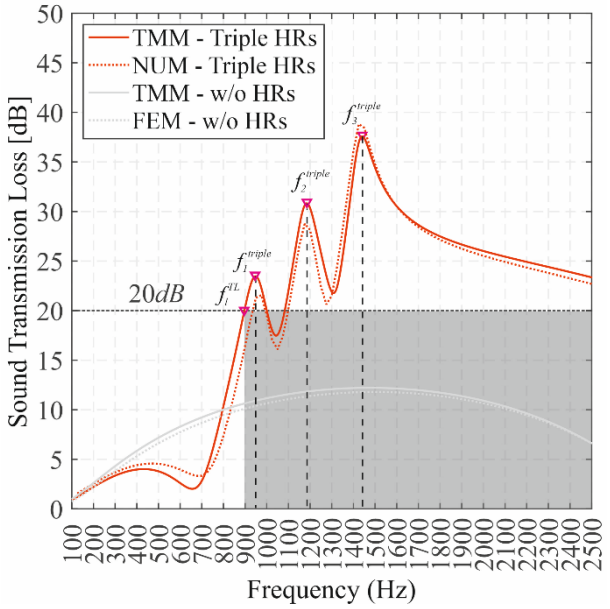

Figure 7. Evaluation of the nSTL for a triple symmetric proposition for three different frequencies $f_1 = 950$ **Hz**, $f_2 = 1200$ **Hz** and $f_3 = 1425$**Hz**. The solid lines represent the TMM results, and the dotted lines the numerical results, respectively.

The findings indicate that the transmission loss peaks can be adjusted to achieve desirable transmission characteristics by varying the geometrical configurations of the HRs. This shows the potential for optimizing the meta-structure's geometry further, intending to broaden frequency bands and increase the amplitude of normal sound transmission loss. Nevertheless, this study already demonstrates that the meta-structure, utilizing the classic HR model coupling, effectively reduces sound transmission within the low to middle frequency range while maintaining compact structural dimensions.

5. CONCLUSIONS

In the present work, a numerical study of the sound transmission characteristics of acoustical metasurface composed by the axial coupling of Helmholtz resonators was presented. The proposition consists of symmetrical and axial coupling of six Helmholtz resonators, working at three conditions, the first, the single HR proposition, consists of the coupling of all the six HRs tuned at the same resonant frequency; enabling a high transmission loss capacity higher than 30dB at the peak of the specified frequency f_{single} = 950Hz; at second, the dual proposition, consisted in achieving two resonance frequency f_1^{dual} = 950 Hz and f_2^{dual} = 1200 Hz, enabling two transmission peaks, around 25dB and 35dB at specified frequencies, respectively. Finally, the third proposition, the transmission loss could be achieved at f_1^{triple}, f_2^{triple}, and f_3^{triple}, in the frequencies, 950Hz, 1200Hz and 1425Hz, respectively.

Another important remark is the implementation of a measurement three-microphone method [8] as an alternative method to the ASTM E2611 [11].

In future works, the aim will be to expand the optimization methods of normal sound transmission loss under normal and diffuse conditions. It is expected that the obtained results demonstrate that the axial coupling resonators are important contributions to the research and development of AMM applications in noise insulation in ventilated system panels.

6. ACKNOWLEDGMENTS

This work is financed by national funds through FCT - Foundation for Science and Technology, under grant agreement UI/BD/150864/2021 attributed to the 1st author, and by FCT / MCTES through national funds (PIDDAC) under the R&D Unit Institute for Sustainability and Innovation in Structural Engineering (ISISE), under reference UIDB/04029/2020, and under the Associate Laboratory Advanced Production and Intelligent Systems ARISE under reference LA/P/0112/2020.

7. REFERENCES

[1] Ramos D, Godinho L, Amado-Mendes P, Mareze P. Broadband low-frequency bidimensional honeycomb lattice metastructure based on the coupling of subwavelength resonators. Appl Acoust 2022;199:109038. https://doi.org/10.1016/j.apacoust.2022.109038.

[2] Jiménez N, Romero-García V, Pagneux V, Groby J-PP. Rainbow-trapping absorbers: Broadband, perfect and asymmetric sound absorption by subwavelength panels for transmission problems. Sci Rep 2017;7:13595. https://doi.org/10.1038/s41598-017-13706-4.

[3] Langfeldt F, Khatokar AJ, Gleine W. Plate-type acoustic metamaterials with integrated Helmholtz resonators. Appl Acoust 2022;199:109019. https://doi.org/10.1016/j.apacoust.2022.109019.

[4] Jo C, Jeong J, Kwon BJ, Park KC, Oh IK. Omnidirectional two-dimensional acoustic cloak by axisymmetric cylindrical lattices. Wave Motion 2015;54:157–69. https://doi.org/10.1016/j.wavemoti.2014.12.004.
[5] Umnova O, Brooke D, Leclaire P, Dupont T. Multiple resonances in lossy acoustic black holes - theory and experiment. J Sound Vib 2023;543:117377. https://doi.org/10.1016/j.jsv.2022.117377.
[6] Sangiuliano L, Reff B, Palandri J, Wolf-Monheim F, Pluymers B, Deckers E, et al. Low frequency tyre noise mitigation in a vehicle using metal 3D printed resonant metamaterials. Mech Syst Signal Process 2022;179:109335. https://doi.org/10.1016/j.ymssp.2022.109335.
[7] Atalla N, Sgard F. Modeling of perforated plates and screens using rigid frame porous models. J Sound Vib 2007;303:195–208. https://doi.org/10.1016/j.jsv.2007.01.012.
[8] Salissou Y, Panneton R, Doutres O. Complement to standard method for measuring normal incidence sound transmission loss with three microphones. J Acoust Soc Am 2012;131:EL216–22. https://doi.org/10.1121/1.3681016.
[9] Johnson DL et al. Theory of dynamic permeability and tortuosity in fluid-saturated porous media. J Fluid Mech 1987;176:379-402.
[10] Champoux Y, Allard JF. Dynamic tortuosity and bulk modulus in air-saturated porous media. J Appl Phys 1991;70:1975–9. https://doi.org/10.1063/1.349482.
[11] ASTM E2611. Standard Test Method for Measurement of Normal Incidence Sound Transmission of Acoustical Materials Based on the Transfer Matrix Method. ASTM Int 2009:1–14. https://doi.org/10.1520/E2611-09.2.